ADVANCED BIOLOGY
www.advanced-bio.com

Peptide Mimics of the Cysteine-Rich Regions of HapX and SreA Bind a [2Fe-2S] Cluster In Vitro

Daniele Rossetto, Lorenzo Sebastianelli, Simon Oberegger, Smilja Todorovic, Hubertus Haas, and Sheref S. Mansy**

HapX and SreA are transcription factors that regulate the response of the fungus *Aspergillus fumigatus* to the availability of iron. During iron starvation, HapX represses genes involved in iron consuming pathways and upon a shift to iron excess, HapX activates these same genes. SreA blocks the expression of genes needed for iron uptake during periods of iron availability. Both proteins possess cysteine-rich regions (CRR) that are hypothesized to be necessary for the sensing of iron levels. However, the contribution of each of these domains to the function of the protein has remained unclear. Here, the ability of peptide analogs of each CRR is determined to bind an iron-sulfur cluster in vitro. UV–vis and resonance Raman (RR) spectroscopies reveal that each CRR is capable of coordinating a [2Fe-2S] cluster with comparable affinities. The iron–sulfur cluster coordinated to the CRR-B domain of HapX displays particularly high stability. The data are consistent with HapX and SreA mediating responses to cellular iron levels through the direct coordination of [2Fe-2S] clusters. The high stability of the CRR-B peptide may also find use as a starting point for the development of new green catalysts.

1. Introduction

Iron is an essential metal for all eukaryotes and most prokaryotes because numerous enzymes of central metabolism rely on an iron cofactor for activity. Consequently, iron plays a central role during infection, as both pathogens and their hosts require iron for survival. However, excess iron is also toxic, as free, unchelated iron ions can lead to oxidative stress through Fenton-like reactions and can compete with non-iron-metal-binding sites.[1,2] Therefore, organisms have evolved sophisticated regulatory pathways to ensure iron homeostasis,[3,4] although key components of such pathways have remained difficult to decipher in detail. For example, the most common airborne mold pathogen for humans, *Aspergillus fumigatus*, exploits two transcription factors, HapX and SreA, within an iron regulatory network, but their mode of iron-sensing is mechanistically unclear.[5] In vivo studies demonstrate that the basic leucine zipper (bZIP)-type transcription factor HapX represses the expression of genes involved in iron consuming pathways during iron starvation and activates these same genes when iron is in excess.[6–8] Moreover, these studies show that HapX is also involved in the activation of high-affinity iron acquisition mechanisms when the supply of iron is limited. The fact that HapX is crucial for adaption to both iron limitation and excess strongly indicates that HapX must be able to sense cellular iron and does so by switching between three different states, including iron deficient, neutral inactive, and iron excess states.[6,7] In comparison, the GATA-type transcription factor SreA, similar to its homologue from *Schizosaccharomyces pombe*, represses high-affinity uptake mechanisms when the iron is plentiful.[9,10] HapX and SreA are connected by a negative transcriptional feedback loop,[11] and the simultaneous inactivation of both is lethal.[12]

HapX and SreA contain sequence motifs that are suggestive of metal-binding. HapX possesses four cysteine-rich regions (CRR), referred to as CRR-A, CRR-B, CRR-C, and CRR-D, while SreA contains a single CRR, herein termed CRR-S (**Table 1**). CRR-A, CRR-B, CRR-C of HapX and CRR-S of SreA contain a CX_2C motif, which is commonly found in [2Fe-2S], [4Fe-4S], and mononuclear $Fe^{2+/3+}$ and Zn^{2+} binding proteins.[13] Of the four HapX CRR domains, CRR-A and CRR-B are the most similar, possessing CX_2C and CXC motifs separated by four and five residues,

D. Rossetto[+], S. S. Mansy
D-CIBIO
University of Trento
via Sommarive 9, Trento 38123, Italy
E-mail: sheref.mansy@ualberta.ca
L. Sebastianelli, S. S. Mansy
Department of Chemistry
University of Alberta
11227 Saskatchewan Drive, Edmonton, Alberta T6G 2G2, Canada
S. Oberegger, H. Haas
Institute of Molecular Biology
Medical University of Innsbruck
Innrain 80, Innsbruck 6020, Austria
E-mail: hubertus.haas@i-med.ac.at
S. Todorovic
Instituto de Tecnologia Química e Biológica António Xavier
Universidade Nova de Lisboa
Av da República, Oeiras 2780-157, Portugal

The ORCID identification number(s) for the author(s) of this article can be found under https://doi.org/10.1002/adbi.202300545

[+]Present address: Max Planck Institute of Molecular Cell Biology and Genetics, Pfotenhauerstraße 108, 01307 Dresden, Germany

DOI: 10.1002/adbi.202300545

Table 1. Peptides used in this study.

name	peptide	motif	Fe^{2+} K_d [μM]
CRR-A	GCNDCSTSHCQCI	CX_2CX_4CXC	20 ± 2
CRR-B	PCGFCSDGTPCICA	CX_2CX_5CXC	40 ± 3
CRR-C	KGCANGPGTCAQCLADPRRTLFCGK	$CX_6CX_2CX_9C$	18 ± 2
CRR-D	GCCGGKGADGGCCG	CCX_8CC	71 ± 5
CRR-S	SCPGGGNCNGTGGAEGCDGCP	$CX_5CX_8CX_2C$	64 ± 9

respectively. CXC motifs have been demonstrated to bind Fe^{2+}, Co^{2+}, and Zn^{2+} with high affinity and to stabilize the formation of [2Fe-2S] clusters.[14] HapX CRR-D contains two consecutive Cys separated by eight residues rather than a CX_2C or CXC sequence. Consecutive metal-binding Cys residues are found in metallothioneins.[15] All of these potential metal-binding sites within A. *fumigatus* HapX and SreA are compact, containing four cysteine residues within a twelve residue stretch for CRR-A, CRR-B, and CRR-D. HapX CRR-C and SreA CRR-S are longer, with motifs spanning 21 and 19 residues, respectively, from the first to the fourth cysteine.

Several lines of evidence indicate that the CRRs of HapX and SreA are necessary to sense the availability of cellular iron. Mutational analysis of cysteine residues revealed that mainly CRR-B, but to a lower degree also CRR-A and even less CRR-C, are required for HapX's role in iron detoxification but not iron starvation.[7] Mutation of CRR-D was phenotypically inconspicuous. These data indicate that at least three of the four HapX CRRs are involved in the sensing of iron excess. Further, the sensing of iron is likely through the formation of [2Fe-2S] clusters. Glutaredoxins mediate the transfer of [2Fe-2S] clusters,[16] and an *A. fumigatus* glutaredoxin homologue GrxD interacts with both HapX and SreA. In vivo studies indicate that GrxD mediates the removal of [2Fe-2S] clusters from both HapX and SreA, which switches HapX from an "iron excess" to an "iron starvation" mode of activity and inactivates SreA.[17] Transcriptional response to iron availability is tied to the synthesis of [2Fe-2S] clusters in the mitochondrion and not to the cytosolic biosynthesis of [4Fe-4S] clusters.[18] Finally, the C-terminal domain of HapX (amino acids 161–491) containing the four CRRs was recombinantly expressed in *Escherichia coli* and showed a UV–vis spectrum indicative of a [2Fe-2S] cluster.[17]

2. Results and Discussion

2.1. Phylogenetic Conservation of HapX and SreA CRRs in Fungi

The high degree of phylogenetic conservation of CRR-B and CRR-S across distantly related fungal species suggested that these CRRs were particularly important for function (**Figure 1**; Figure S1, Supporting Information). Protein BLAST (BlastP) searches with the FungiDB and NCBI databases, which included all fungal divisions, revealed that CRR-B was conserved in the fungal divisions Ascomycota and Basidiomycota but not in Blastocladiomycota, Chytridiomycota, and Mucoromycota. However, CRR-B was not conserved in the Ascomycota classes Pneumocystidomycetes and Schizosaccharomycetes and the Basidiomycota classes Pucciniomycetes and Tremellomycetes. The other HapX

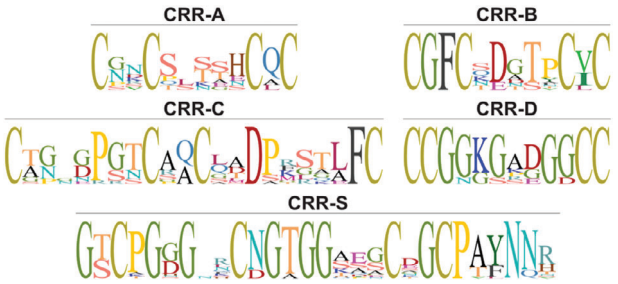

Figure 1. Consensus sequences of the CRRs of HapX and SreA. Multiple alignment of CRRs are in Figure S1 (Supporting Information).

CRRs showed lower phylogenetic conservation with CRR-C being more frequently employed than CRR-A and CRR-D. SreA and the CRR of SreA, i.e., CRR-S, were found to be even more conserved than HapX CRR-B. CRR-S was present in all fungal divisions but Chytridiomycota, which possess SreA homologues lacking typical CRRs. Within these divisions, SreA and CRR-S were identified in all classes except for the Ascomyctes class Taphrinomycetes. Importantly, conservation included the cysteine residues thought to be necessary for the coordination of a [2Fe-2S] cluster in addition to other residues that may play a role in the transfer or stability of the iron-sulfur cluster.

2.2. Peptide Mimics of CRRs

To circumvent the need to produce soluble and functional protein that can be interrogated in vitro and to facilitate the analysis of the individual characteristics of each potential iron-sulfur cluster-binding domain of HapX and SreA, peptide analogues were synthesized and either incubated with a Co^{2+} probe or with Fe^{3+} and HS^- under anaerobic conditions. Such an approach builds on prior experience with small, cysteine-containing peptides (2–25 residues in length) that coordinate iron-sulfur clusters.[14,19–22] Peptide analogs of iron–sulfur motifs found in proteins frequently retain the ability to coordinate their cognate iron–sulfur cluster.[23] Here, each synthesized peptide was identical in sequence to a region within HapX or SreA, with the exception of HapX CRR-C (Table 1). As the 23-residue CRR-C peptide was not soluble in aqueous solution, single lysine residues were added to both N- and C-termini, which gave rise to a soluble 25-residue peptide. AlphaFold predicts that these CRR domains reside within largely unstructured regions of the protein.

2.3. UV–vis Spectra of CRR Peptides are Consistent with Metal Binding

To determine if the cysteinyl side chains of the peptides were properly organized to bind a thiophilic metal ion, the binding of Co^{2+} was investigated. Co^{2+} is a useful spectroscopic probe of iron-binding sites,[24] since the resulting UV–vis spectra are easily interpretable in terms of the number of ligating thiolates. All five samples showed an electronic transition at ≈750 nm, indicative of four thiolates coordinated to the Co^{2+},[24] as would be expected for an iron–sulfur binding motif (Figure S2, Supporting Information). To ensure that all four thiolates were provided by

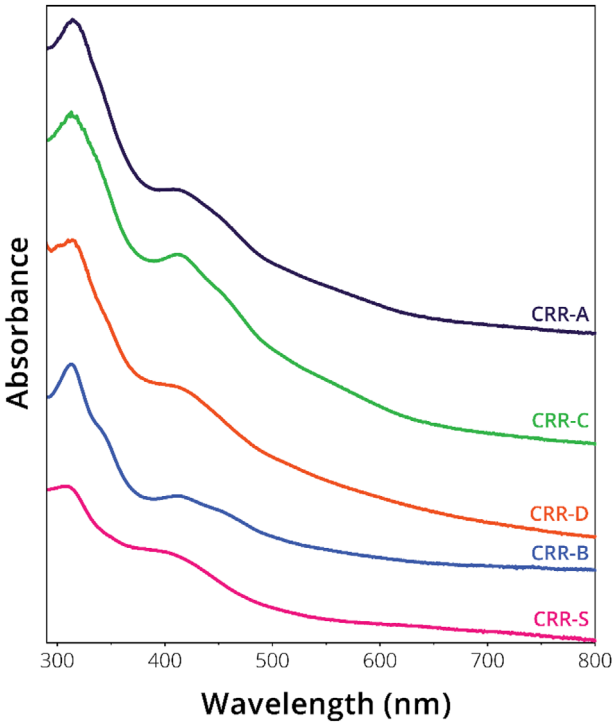

Figure 2. UV–vis spectra of $[2Fe\text{-}2S]^{2+}$ CRR peptides of HapX and SreA. Iron–sulfur clusters were synthesized with 5 mM peptide, 2.5 mM Fe^{3+}, 2.5 mM HS^- in 20 mM glycylglycine, pH 8.7, then diluted fivefold to collect the UV–vis spectra. An unstacked version of the data is shown in Figure S11 (Supporting Information).

a single peptide, the stoichiometry of Co^{2+} complexed with CRR-B was further investigated. After correcting for the purity of the sample (Tables S1 and S2, Supporting Information), the method of continuous variation indicated a stoichiometry of 1:1 for Co^{2+} and CRR-B (Figure S3, Supporting Information). After confirming that each peptide was capable of the tetrahedral coordination of a metal ion, the peptides were titrated with Fe^{2+} instead of Co^{2+}. The addition of Fe^{2+} to each peptide gave UV–vis absorption spectra of a mononuclear iron center with absorbance peaks near 315 and 345 nm (Figure S4, Supporting Information). The data were fit to the Hill equation to determine dissociation constants (Table 1; Figures S5–S9, Supporting Information), which were similar to values obtained previously with a 25 residue peptide that contained four cysteine residues within a region that possessed CXC and CX_2C motifs separated by 16 residues.[14]

To evaluate the ability of each peptide to stabilize the formation of an iron-sulfur cluster, 5 mM of each peptide was either incubated with 2.5 or 5 mM Fe^{3+} and HS^-. In each case, UV–vis spectra showed characteristic bands at ≈415 and ≈450 nm (**Figure 2**; Figures S10 and S11, Supporting Information) indicative of a [2Fe-2S] cluster. Under these conditions, free peptide was always present. Although it was not possible to definitively determine the number of peptides coordinated to each [2Fe-2S] cluster, the Co^{2+} data were consistent with a 1:1 stoichiometry (as described above), indicating that the four peptidyl Cys were spatially arranged in a way to bind a single metallocofactor. To gain insight into the stability of the iron–sulfur cluster coordinated to each peptide, aliquots were incubated at 50 °C and the change in absorbance at 415 nm was monitored by UV–vis spectroscopy. The clusters formed by CRR-C and CRR-D were the least stable, completely degrading within 30 min at 50 °C (Figure S12, Supporting Information), forming visible precipitate. [2Fe-2S] CRR-B was the most stable, surviving for ≈53 h at 50 °C. In fact, the [2Fe-2S] cluster coordinated to CRR-B was so stable that the cluster was still present at room temperature over one year after synthesis (Figure S13, Supporting Information). Changes to the spectra over time likely reflected a combination of maturation and degradation, with the latter leading to the formation of iron hydroxide precipitates that altered the baseline. Also, the extinction coefficient of mononuclear, rubredoxin-like centers and [2Fe-2S] clusters are different,[25] leading to increases and decreases in intensity depending on whether [2Fe-2S] clusters are being formed or lost, respectively. The [2Fe-2S] clusters assembled on CRR-A and CRR-S showed comparable stability, with lifetimes of ≈17 and 21 h, respectively, at 50 °C (Figure S12, Supporting Information).

2.4. Resonance Raman Spectroscopy Confirms the Presence of a $[2Fe\text{-}2S]^{2+}$ Cluster

The nature of the iron–sulfur cluster was confirmed for each peptide by resonance Raman (RR) spectroscopy, which can sensitively reveal the type of iron–sulfur cluster and the ligands to the cluster.[26] All spectra were measured under strictly anaerobic conditions, employing 458 nm laser excitation that matched the S → Fe ligand to metal charge transfer (LMCT) electronic transition of the cluster. Under these conditions, RR spectra comprised selectively enhanced Fe—S modes originating preferentially from bridging $(Fe—S)^b$ and terminal $(Fe—S)^t$ vibrational modes, derived from inorganic S and cysteinyl S ligands, respectively. The frequencies of the so-called maker bands, which are characteristic for the cluster type, were found between 281–291 cm^{-1} in all herein studied peptides, regardless of the peptide:Fe^{3+}:S^- stoichiometry (**Figure 3**; Figure S14, Supporting Information). This RR mode at <300cm^{-1} was indicative of an all-cysteinyl coordinated $[2Fe\text{–}2S]^{2+}$ cluster (e.g., $[3Fe\text{–}4S]^+$ and cubane $[4Fe\text{–}4S]^{2+}$ possess characteristic RR bands at ≈346 and ≈333 cm^{-1}, respectively). The best resolved spectra, most likely indicating the most homogeneous and symmetric structure, originated from CRR-B, with $[2Fe\text{-}2S]^t$ at 286 cm^{-1} and additional bands consistent with a [2Fe–2S] cluster ($[2Fe\text{–}2S]^t$ modes at 340 and 357 cm^{-1}, and $[2Fe\text{–}2S]^b$ at 395 cm^{-1}) (Figure 3), which were comparable to those of some previously investigated [2Fe-2S] containing ferredoxins.[27] Note that the RR spectra of peptides CRR-A, -C, -D, and -S appeared more heterogeneous, with broader overlapping bands (Figure 3; Figure S14, Supporting Information). Nevertheless, in all cases, the presence of a well resolved band at 280–291 cm^{-1} unambiguously indicated the formation of a $[2Fe\text{-}2S]^{2+}$ cluster. This was further confirmed by component analysis in which the experimental RR spectra were fit to individual vibrational components, revealing essentially the same band frequencies with different relative intensity ratios and widths (Figures S15–S17 and Table S3, Supporting Information). That is, component analysis demonstrated that all peptides reported here coordinated a [2Fe-2S] cluster under all conditions tested that possessed Fe^{3+} and HS^- and did not indicate the presence of either a [3Fe-4S] or

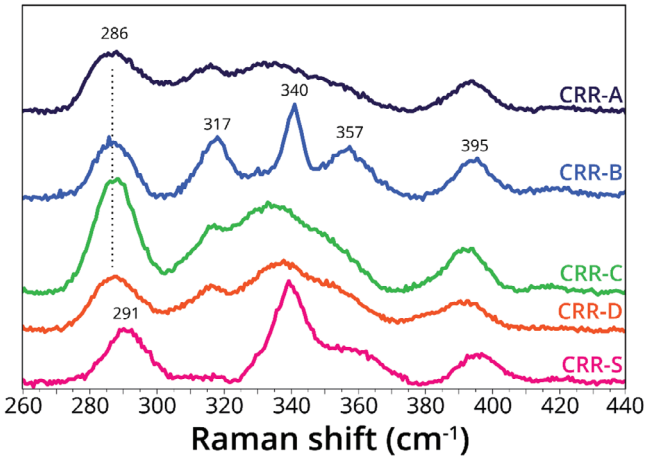

Figure 3. Resonance Raman spectra of the HapX and SreA CRR peptides. Spectra of 5 mM peptides in the presence of 5 mM Fe^{3+}, 5 mM HS^- and 20 mM glycylglycine, pH 8.7, measured with 458 nm excitation and a laser power of 3–5 mW at −190 °C. The corresponding UV–vis spectra of each sample are shown in Figure S10 (Supporting Information). Deconvoluted spectra of CRR-A, CRR-B and CRR-S are shown in Figure S16–S18 (Supporting Information) (top traces). Tentative assignments of vibrational modes, frequencies and widths obtained by component analysis are provided in Table S3 (Supporting Information).

[4Fe-4S] cluster. However, we cannot completely exclude the possibility that traces of $Fe(Cys)_4$ centers, analogous to that found in rubredoxin, were present in CRR-A-D since the symmetric Fe-S(Cys) stretch coincides with an ice vibrational mode observed in the control spectrum (Figure S15 and Table S3, Supporting Information). Interestingly, small differences in the frequency of the $[2Fe\text{-}2S]^t$ modes of the CRRs of HapX and SreA indicated a slightly stronger Fe—S bond in the latter.

3. Conclusion

Iron homeostasis depends on a sophisticated balancing of iron acquisition, consumption, and detoxification. In the mold *A. fumigatus*, this equilibrium is mediated, in large part, by transcriptional regulation through the transcription factors HapX and SreA.[5] However, because of the size and complexity of these proteins, the contribution of each CRR remained unclear. The only available X-ray crystal structure of HapX was of a truncated protein that lacked CRRs,[28] and no crystal structure of SreA has been reported. Now, by UV–vis and RR spectroscopies, we have shown that peptide mimics of CRR-A, -B, -C, -D, and -S are all capable of coordinating a [2Fe-2S] cluster in vitro and could do so without the aid of other regions of the protein. These results suggest that CRR homologues within other organisms are likely capable of binding [2Fe-2S] clusters. The particularly high stability of the [2Fe-2S] cluster of CRR-B is consistent with the importance of this domain in mediating the activity of HapX.[7] In the absence of structural information, it is difficult to identify the chemical reasons for this stability. However, the sequence motif is consistent with the binding of a [2Fe-2S] cluster,[13] the presence of Pro residues likely enhances structural stability, and a Pro residue immediately following a ligating Cys was shown to increase the affinity of a dipeptide for Fe^{2+}.[29] The next most stable [2Fe-2S] CRR of HapX is that of CRR-A, a domain previously found to significantly influence response to iron excess in *A. fumigatus*.[7] Out of the four CRRs of HapX, CRR-C and CRR-D peptides possess the least stable [2Fe-2S] clusters in vitro. CRR-C more weakly affects the activity of HapX in vivo, and the role of CRR-D has been less thoroughly investigated.

Although our data on single peptides cannot be interpreted in terms of precise functional roles within their corresponding protein domains, the differences in [2Fe-2S] stability for CRR-A, -B, -C, and CRR-D peptides may indicate that the loading of the different CRRs within HapX depends on the cellular availability of [2Fe-2S] clusters. That is, the differing propensities to coordinate a [2Fe-2S] cluster may lead to cumulative occupancies that regulate transitions between HapX in the iron starvation, neutral inactive, and iron excess states.[6,7] Since the stability of the [2Fe-2S] cluster coordinated to the CRR-S peptide is similar to that of CRR-C, a domain previously demonstrated to significantly impact the response of HapX to iron,[7] the activity of SreA may also rely on the coordination of a [2Fe-2S] to the CRR-S domain. Despite the limitations of probing the in vivo characteristics of proteins by investigating peptide analogues in vitro, the ability of each CRR peptide to coordinate a [2Fe-2S] cluster, as we show here, adds to a growing body of evidence that iron-responsive transcriptional regulation in *A. fumigatus* is mediated by the coordination of [2Fe-2S] clusters to CRR domains. Additionally, the high stability of the iron-sulfur cluster coordinated to CRR-B suggests that artificial metallopeptide catalysts inspired by the active sites of metalloenzymes could be designed for applications, such as carbon fixation,[29] that help mitigate climate change.

We would like to note that care should be taken to not overinterpret the data presented here. Although data from small peptides likely probe well the impact of the primary sequence encompassing the ligands to the iron–sulfur cluster, particularly for a flexible domain that may be unstructured in the absence of cognate metal, as is often the case for metal trafficking machinery,[22,30] we cannot rule out the possibility that the affinities for iron and [2Fe-2S] clusters might be different in the full-length protein. Small peptides cannot fully mimic the local environment within a large, 3D protein.[31] Moreover, metal affinities and selectivities observed in vitro do not necessarily indicate biological relevance.[32] In a cell, selectivity for the required metal ion is largely controlled by availability and targeted delivery,[33] factors not probed here. Investigations of iron-sulfur clusters are impacted by these same considerations. The same motifs that bind iron–sulfur clusters can also bind Zn^{2+} with high affinity.[13] In fact, iron and zinc homeostasis are likely linked in *A. fumigatus*.[34,35] What is clear from our studies is that the primary sequence encompassing the CRR domains can bind an iron–sulfur cluster. More work is needed to tie this observation to activity in vivo.

4. Experimental Section

All reagents were purchased form Merck (Darmstadt, Germany) or Fisher Scientific (Nepean, Canada) and used without further purification. Unless otherwise specified, all reactions were carried out at room temperature under anoxic conditions (<1 ppm O_2) inside a Genesis Glovebox System (Vacuum Atmosphere Company, USA). All solutions were prepared using deoxygenated water that was distilled under N_2.

Peptide Synthesis: Peptides were synthesized by solid phase peptide synthesis, as previously described.[14] *N,N*-dimethyl formamide (DMF)

was used as the solvent and Wang resin was used as the starting polymeric support. The building blocks employed were trityl-protected Fmoc-cysteine (Fmoc-Cys(Trt)-OH) and tert-butyl (OtBu) side chain-protected Fmoc-α-amino acids. Elongation of the peptide chain occurred through sequential Fmoc deprotection of the residue attached to the resin and Fmoc-AA-OH coupling. Fmoc deprotection was achieved by rinsing the mixture with a 20% (v/v) piperidine solution in DMF. For each coupling, an excess of Fmoc-α-amino acid derivative (Fmoc-AA-OH:anchored AA, 4:1) was added to the resin. With the exception of Fmoc-Cys(Trt)-OH, Fmoc-α-amino acid derivatives were activated using a combination of hydroxybenzotriazole (HOBt), *N,N,N′,N′*-tetramethyl-O-(benzotriazol-1-yl)uronium tetrafluoroborate (TBTU), and *N,N*-diisopropylethylamine (DIPEA). Fmoc-Cys(Trt)-OH was activated using a mixture of *N,N′*-diisopropylcarbodiimide (DIC) and HOBt. Upon completion of the synthesis, the polymers were detached from the resin and deprotected by treatment with a solution consisting of trifluoroacetic acid (TFA), water, triisopropylsilane (TIS), and 1,2-ethanedithiol (EDT) in a ratio of 97:1:1:1 (v/v) for 2 h. The resulting product was precipitated using a cold diethyl ether/petroleum ether mixture (30:70, v/v), followed by washing cycles with diethyl ether. The peptides were then solubilized in 20% acetic acid (v/v), rapidly frozen in liquid nitrogen, and subsequently lyophilized overnight at −84 °C using a Labconco FreeZone Freeze Dryer.

Synthesis of [2Fe-2S] Clusters: Each peptide (1 or 5 mM) in glycylglycine (20 mM) was pH adjusted to 8.7 in anaerobic conditions. Freshly prepared solutions of $FeCl_3$ and Na_2S were added to the peptide solutions to a final peptide:Fe^{3+}:HS^- molar ratio of 2:1:1 or 1:1:1. For UV–vis experiments, the solutions were immediately transferred to quartz cuvettes. For RR experiments, the solutions were incubated for 4 h at room temperature before freezing with liquid N_2.

UV–vis Spectra and Affinity Measurements: UV–vis spectra of the samples were recorded inside a glovebox with a Genesys 150 UV–vis spectrophotometer (ThermoFisher) with an integration time of 0.5 s and an interval of 1 nm. Binding affinity was calculated as previously described.[14,36] Briefly, the peptide solutions were prepared under anoxic conditions by dissolving the peptides (1 mM) in 20 mM glycylglycine at pH 8.7. This pH was chosen to ensure that all the thiols in the peptide would be deprotonated and available for the binding of an iron–sulfur cluster. The intracellular pH of *A. fumigatus* is lower.[37] Spectra were collected after each addition of metal and the absorbance at 750 nm was fit with GraphPad Prism v. 6.00 (GraphPad Software, La Jolla Californiaa USA) to the following equation: (1) y = BMax××h /(Kdh + xh), where BMax was the absorbance reached at saturation, and h was the Hill slope.

Resonance Raman spectroscopy: Resonance Raman (RR) spectra were acquired with Raman spectrometer (LabRAM 800 HR, Jobin Yvon) equipped with a 1200 lines mm^{-1} grating and a liquid-nitrogen-cooled CCD detector. An Olympus 20X objective was used for laser focusing onto the sample and light collection in the backscattering geometry. Spectra were measured (458 nm excitation, Argon ion laser, Coherent Innova 90c) from 2 µL aliquots of the CRR peptides (5 mM) placed onto a microscope stage (THMS 600, Linkham) under anaerobic conditions, which was cooled to 77 K with liquid N_2. Experiments were performed using 3–5 mW laser power and an accumulation time of 60 s; 4–10 spectra were co-added in each measurement to improve the signal to noise ratio. All spectra were subjected to polynomial baseline subtraction; the frequencies and widths of RR bands were determined by component analysis using LabSpec software.

Phylogenetic Analysis: Multiple alignment of CRRs and their consensus sequences was with Geneious Prime 2023.0.4 (https://www.geneious.com).

Method of Continuous Variation: In an anaerobic environment, two separate parental solutions of the CRR-B peptide and $CoCl_2$ were prepared in 0.1 M glycylglycine, pH 8.7. Once a series of quartz cuvettes were conditioned with N_2 gas, aliquots of the $CoCl_2$ and peptide solutions were mixed and diluted with 0.1 M glycylglycine, pH 8.7 directly to a final total concentration of Co^{2+} and CRR-B of 1 mM. The mixing of the two parental solution was done in a way to produce samples at molar fractions of Co^{2+} that were evenly spaced from 0.1 to 0.95. The resulting solutions were left to equilibrate for 5 min. Subsequently, full spectra from 200 to 1000 nm were recorded with an Agilent Cary 3500 UV–vis spectrophotometer.

Elemental Analysis: A sample of solid CRR-B was analyzed with a Thermo Flash 2000 Elemental Analyzer for CHNS. Analysis was performed by the Analytical and Instrumentation Laboratory of the department of chemistry of the University of Alberta.

Statistical Analysis: All RR spectra were subjected to polynomial baseline substraction. Frequencies and widths of RR bands were determined by component analysis using LabSpec software (HORIBA France SAS). Saturation binding analysis of the data was performed with GraphPad Prism version 6.0 (GraphPad Software, La Jolla, CA, U.S.A.). Data with error bars (Figures S5–S9, Supporting Information) are represented as median ± SD with n = 3 replicates for each experiment. For the method of continuous variation (Figure S3, Supporting Information), R^2 is reported for the fitting. Measured values for the elemental composition of the sample reported in Tables S1 and S2 (Supporting Information) are the average of n = 3 independent measurements.

Supporting Information

Supporting Information is available from the Wiley Online Library or from the author.

Acknowledgements

SSM acknowledges support from the Simons Foundation [290358FY18 and 290358FY19] and the Natural Sciences and Engineering Research Council of Canada (NSERC) [RGPIN-2020-04375 to S.S.M.]. HH and SSM thank the Euregio Science Fund [IPN95] for financial support. The authors thank COST Action 15 133: "The Biogenesis of Iron-sulfur Proteins: from Cellular Biology to Molecular Aspects" (FeSBioNet; www.cost.eu/actions/CA15133), supported by COST (European Cooperation in Science and Technology). This work was also supported by FCT – Fundação para a Ciência e a Tecnologia, I.P., through MOSTMICRO-ITQB R&D Unit [UIDB/04612/2020, UIDP/04612/2020] and LS4FUTURE Associated Laboratory [LA/P/0087/2020]. HH acknowledges support by FWF DOC82.

Conflict of Interest

The authors declare no conflict of interest.

Data Availability Statement

The data that support the findings of this study are openly available in Zenodo at [DOI: 10.5281/zenodo.10656386], reference number [1].

Keywords

A. fumigatus, cysteine rich region, iron homeostasis, iron–sulfur cluster, metallopeptide, peptide mimics

Received: October 9, 2023
Revised: February 7, 2024
Published online: April 4, 2024

[1] C. C. Winterbourn, *Toxicol. Lett.* **1995**, *82–83*, 969.
[2] Y. Kohgo, K. Ikuta, T. Ohtake, Y. Torimoto, J. Kato, *Int. J. Hematol.* **2008**, *88*, 7.
[3] N. Nelson, *EMBO J.* **1999**, *18*, 4361.

[4] S. C. Andrews, A. K. Robinson, F. Rodríguez-Quiñones, *FEMS Microbiol. Rev.* **2003**, *27*, 215.
[5] M. Misslinger, P. Hortschansky, A. A. Brakhage, H. Haas, *Biochim. Biophys. Acta – Mol. Cell Res.* **2021**, *1868*, 118885.
[6] M. Schrettl, N. Beckmann, J. Varga, T. Heinekamp, I. D. Jacobsen, C. Jöchl, T. A. Moussa, S. Wang, F. Gsaller, M. Blatzer, E. R. Werner, W. C. Niermann, A. A. Brakhage, H. Haas, *PLoS Pathog.* **2010**, *6*, e1001124.
[7] F. Gsaller, P. Hortschansky, S. R. Beattie, V. Klammer, K. Tuppatsch, B. E. Lechner, N. Rietzschel, E. R. Werner, A. A. Vogan, D. Chung, U. Mühlenhoff, M. Kato, R. A. Cramer, A. A. Brakhage, H. Haas, *EMBO J.* **2014**, *33*, 2261.
[8] T. Furukawa, M. T. Scheven, M. Misslinger, C. Zhao, S. Hoefgen, F. Gsaller, J. Lau, C. Jöchl, I. Donaldson, V. Valiante, A. A. Brakhage, M. J. Bromley, H. Haas, P. Hortschansky, *Nucleic Acids Res.* **2020**, *48*, 3567.
[9] M. Schrettl, H. S. Kim, M. Eisendle, C. Kragl, W. C. Nierman, T. Heinekamp, E. R. Werner, I. Jacobsen, P. Illmer, H. Yi, A. A. Brakhage, H. Haas, *Mol. Microbiol.* **2008**, *70*, 27.
[10] B. Pelletier, A. Trott, K. A. Morano, S. Labbé, *J. Biol. Chem.* **2005**, *280*, 25146.
[11] M. Schrettl, H. Haas, *Curr. Opin. Microbiol.* **2011**, *14*, 400.
[12] H. Haas, *Nat. Prod. Rep.* **2014**, *31*, 1266.
[13] L. Belmonte, S. S. Mansy, *J. Chem. Inf. Model.* **2017**, *57*, 3162.
[14] L. Valer, D. Rossetto, T. Parkkila, L. Sebastianelli, G. Guella, A. L. Hendricks, J. A. Cowan, L. Sang, S. S. Mansy, *ChemBioChem* **2022**, *24*, 202200202.
[15] P. Coyle, J. C. Philcox, L. C. Carey, A. M. Rofe, *Cell. Mol. Life Sci.* **2002**, *59*, 627.
[16] E. A. Talib, C. E. Outten, *Biochim. Biophys. Acta – Mol. Cell Res.* **2021**, *1868*, 118847.
[17] M. Misslinger, M. T. Scheven, P. Hortschansky, M. S. López-Berges, K. Heiss, N. Beckmann, T. Heigl, M. Hermann, T. Krüger, O. Kniemeyer, A. A. Brakhage, H. Haas, *PLoS Genet.* **2019**, *15*, e1008379.
[18] M. Misslinger, B. E. Lechner, K. Bacher, H. Haas, *Metallomics* **2018**, *10*, 1687.
[19] J. D. Kim, D. H. Pike, A. M. Tyryshkin, G. V. T. Swapna, H. Raanan, G. T. Montelione, V. Nanda, P. G. Falkowski, *J. Am. Chem. Soc.* **2018**, *140*, 11210.
[20] W. Qi, J. Li, C. Y. Chain, G. A. Pasquevich, A. F. Pasquevich, J. A. Cowan, *J. Am. Chem. Soc.* **2012**, *134*, 10745.
[21] C. Bonfio, L. Valer, S. Scintilla, S. Shah, D. J. Evans, L. Jin, J. W. Szostak, D. D. Sasselov, J. D. Sutherland, S. S. Mansy, *Nat. Chem.* **2017**, *9*, 1229.
[22] Y. Liu, S. Liu, A. Tomar, F. S. Yen, G. Unlu, N. Ropek, R. A. Weber, Y. Wang, A. Khan, M. Gad, J. Peng, E. Terzi, H. Alwaseem, A. E. Pagano, S. Heissel, H. Molina, B. Allwein, T. C. Kenny, R. L. Possemato, L. Zhao, R. K. Hite, E. V. Vinogradova, S. S. Mansy, K. Birsoy, *Science* **2023**, *382*, 820.
[23] B. R. Gibney, S. E. Mulholland, F. Rabanal, P. L. Dutton, *Proc. Natl. Acad. Sci. USA* **1996**, *93*, 15041.
[24] A. Nomura, Y. Sugiura, *Inorg. Chem.* **2002**, *41*, 3693.
[25] L. Valer, D. Rossetto, S. Scintilla, Y. J. Hu, A. Tomar, S. Nader, I. O. Betinol, S. S. Mansy, *Can. J. Chem.* **2022**, *100*, 475.
[26] G. Caserta, L. Zuccarello, C. Barbosa, C. M. Silveira, E. Moe, S. Katz, P. Hildebrandt, I. Zebger, S. Todorovic, *Coord. Chem. Rev.* **2022**, *452*, 214287.
[27] S. Todorovic, M. Teixeira, *J. Biol. Inorg. Chem.* **2018**, *23*, 647.
[28] E. M. Huber, P. Hortschansky, M. T. Scheven, M. Misslinger, H. Haas, A. A. Brakhage, M. Groll, *Structure* **2022**, *30*, 934.
[29] L. Belmonte, D. Rossetto, M. Forlin, S. Scintilla, C. Bonfio, S. S. Mansy, *Phys. Chem. Chem. Phys.* **2016**, *18*, 20104.
[30] T. A. Ramelot, J. R. Cort, S. Goldsmith-Fischman, G. J. Kornhaber, R. Xiao, R. Shastry, T. B. Acton, B. Honig, G. T. Montelione, M. A. Kennedy, *J. Mol. Biol.* **2004**, *344*, 567.
[31] S. M. Gutenthaler, S. Tsushima, R. Steudtner, M. Gailer, A. Hoffmann-Röder, B. Drobot, L. J. Daumann, *Inorg. Chem. Front.* **2022**, *9*, 4009.
[32] J. Xu, J. A. Cotruvo, *ACS Bio. Med. Chem. Au* **2022**, *2*, 376.
[33] D. A. Capdevila, K. A. Edmonds, D. P. Giedroc, *Essays Biochem.* **2017**, *61*, 177.
[34] H. Toledo, C. I. Sánchez, L. Marín, J. Amich, J. A. Calera, *Environ. Microbiol.* **2022**, *24*, 643.
[35] R. Vicentefranqueira, F. Leal, L. Marín, C. I. Sánchez, J. A. Calera, *Environ. Microbiol.* **2019**, *21*, 2787.
[36] I. Jarmoskaite, I. Alsadhan, P. P. Vaidyanathan, D. Herschlag, *Elife* **2020**, *9*, e57264.
[37] T. Bagar, K. Altenbach, N. D. Read, M. Benčina, *Eukaryot. Cell* **2009**, *8*, 703.

